JSHC
Japan Society of
Histochemistry and Cytochemistry
Established 1959

Acta Histochem. Cytochem. 47 (3): 113–123, 2014
doi: 10.1267/ahc.14004

Immunocytochemical Localization of Calbindin D28K, Calretinin, and Parvalbumin in Bat Superior Colliculus

Se-Jin Jeong[1], Hyun-Ho Kim[1], Won-Sig Lee[1] and Chang-Jin Jeon[1]

[1]Department of Biology, School of Life Sciences, BK21 Plus KNU Creative BioResearch Group, College of Natural Sciences, and Brain Science and Engineering Institute, Kyungpook National University, Daegu, 702–701, South Korea

Received January 24, 2014; accepted April 28, 2014; published online June 26, 2014

The purpose of this study was to investigate the localization of cells containing the calcium-binding proteins (CBPs) calbindin D28K (CB), calretinin (CR), and parvalbumin (PV) in the superior colliculus (SC) of the bat using immunocytochemistry. CB-immunoreactive (IR) cells formed a laminar tier within the upper superficial gray layer (SGL), while CR-IR cells were widely distributed within the optic layer (OL). Scattered CR-IR cells were also found within the intermediate gray, white, and deep gray layers. By contrast, PV-IR cells formed a laminar tier within the lower SGL and upper OL. Scattered PV-IR cells were also found throughout the intermediate layers, but without a specific laminar pattern. The CBP-IR cells varied in size and morphology: While most of the CB-IR cells in the superficial layers were small round or oval cells, most CR-IR cells in the intermediate and deep layers were large stellate cells. By contrast, PV-IR cells were small to large in size and included round or oval, stellate, vertical fusiform, and horizontal cells. The average diameters of the CB-, CR-, and PV-IR cells were 11.59, 17.17, and 12.60 μm, respectively. Double-immunofluorescence revealed that the percentage of co-localization with GABA-IR cells was 0.0, 0.0, and 10.27% of CB-, CR-, and PV-IR cells, respectively. These results indicate that CBP distribution patterns in the bat SC are unique compared with other mammalian SCs, which suggest functional diversity of these proteins in visually guided behaviors.

Key words: calbindin D28K, calretinin, parvalbumin, immunocytochemistry, superior colliculus

I. Introduction

It is a widely held misunderstanding that bats are blind. In general, bats are better known for echolocation rather than for visual abilities, and there are a large number of studies on the bat's ability to use echolocation [32, 54, 56]. However, bats have two eyes and some visual capabilities; functional opsin genes, which are associated with vision, have been identified recently in some species of bats [64].

Bats can be classified into two main groups: *Megachiroptera* (megabats; about 200 species found throughout Asia, Africa, and Australasia) and *Microchiroptera* (microbats; about 800 species found throughout the world). Megabats, commonly known as fruit bats, have large, frontally positioned eyes, remarkable eyesight, and navigate using highly developed vision and olfaction [25, 61]. In contrast, microbats have small eyes, poor eyesight, and detect prey by echolocation [46, 60]. The greater horseshoe bat, *Rhinolophus ferrumequinum*, has traditionally been included in the group of microbats. This insectivorous species is mainly cave-dwelling and uses echolocation capabilities like other microbats [19, 31]. However, the functional organization of the central visual system in microbats is poorly understood [2, 30, 35].

Among the many calcium-binding proteins (CBPs), there are known to be present in distinct subpopulations of neurons in the central nervous system: calbindin D28K

Correspondence to: Prof. Chang-Jin Jeon, Ph.D., Department of Biology, College of Natural Sciences, Kyungpook National University, 1370 Sankyuk-dong, Daegu, 702–701, South Korea. E-mail: cjjeon@knu.ac.kr

(CB), calretinin (CR), and parvalbumin (PV) [5]. CB was originally described as a prominent cytosolic vitamin D-dependent CBP in the intestine and kidney [62]. CR, a 29 kDa CBP, was first isolated as a cDNA clone from the chick retina [51]. PV, a low molecular-weight protein, was the first CBP to be isolated from the skeletal muscle of lower vertebrates [22]. These three EF-hand CBPs may simply function as calcium buffers, or they may actively participate in calcium-mediated signal transduction [49, 52]. Although the exact functions of these proteins have not been established, CBPs have been used as valuable markers to distinguish different neuronal subpopulations [5, 11] and functional defects in these particular proteins are associated with various neurological disorders [4, 7, 10, 14, 23, 41, 49, 50, 52, 55].

The superior colliculus (SC) is known to be the visuo-motor integration area and controls head, eye, and ear movements. The SC, located below the thalamus, is a laminated component of the midbrain. Within this structure, three superficial layers (zonal, ZL; superficial gray, SGL; and optic layers, OL) receive major inputs from the retina and visual cortex, and are exclusively involved in vision. In contrast, the four deeper layers (intermediate gray, IGL; intermediate white, IWL; deep gray, DGL; and deep white layers, DWL) receive auditory, somatic, and visual input from numerous cortical and subcortical areas involved in head, eye, and ear movements [18, 20, 27]. One of the main organizing features of the SC is the topographical segregation of its afferent fibers and efferent cells, showing specific laminae, clusters, puffs, lattices, and patches [18, 20, 27]. The distribution patterns of CBPs exhibit horizontal laminar segregation in the SC. CB is found in cells that are located in three layers of the mammalian SC [8, 40, 43, 44, 53], while PV-immunoreactive (IR) cells are concentrated in a dense tier within the deep SGL and upper OL [12, 45]. By contrast, CR forms a dense plexus of IR fibers in the superficial layers of the SC [15, 26, 40, 57]. However, there are some species differences in the distribution patterns of CBPs in the SC [29].

Previously, we reported on the distribution pattern of AII amacrine cells in the retina and the central visual system of the greater horseshoe bat *R. ferrumequinum* [30] along with photoreceptor distribution pattern [35]. These reports, along with others [58], demonstrate that cellular organization in the bat retina is well developed suggesting that this organization may also apply to other areas related to vision. In order to better understand the central visual system of the greater horseshoe bat, we aimed to identify CBP-containing cells in the bat SC, characterize these cells morphologically, and investigate whether these CBPs were present in GABAergic interneurons. There are no reports to date that describe the distribution pattern of CBP-containing cells in the SC of any bat. Thus, this study provides basic information about the cellular architecture of the bat SC; the findings reported here contribute significantly to the understanding of bat visuo-motor behavior.

II. Materials and Methods

Animals and tissue preparation

Adult greater horseshoe bats *R. ferrumequinum* were used in this study. The bats were anesthetized with a mixture of ketamine hydrochloride (30–40 mg/kg) and xylazine (3–6 mg/kg) before perfusion. All bats were perfused intracardially with 4% paraformaldehyde and 0.3–0.5% glutaraldehyde in 0.1 M sodium phosphate buffer (pH 7.4) containing 0.002% calcium chloride. Following a pre-rinse with approximately 30 ml of phosphate-buffered saline (PBS, pH 7.4) over a period of 3–5 min, each bat was perfused with 30–50 ml of fixative for 20–30 min via a syringe needle inserted into the left ventricle and aorta. The head was then removed and placed in the fixative for 2–3 hr. The brain was removed from the skull, stored for 2–3 hr in the same fixative, and left overnight in 0.1 M phosphate buffer (pH 7.4) containing 8% sucrose and 0.002% $CaCl_2$. The SC was removed, mounted onto a chuck, and cut into 50 μm thick coronal sections with a Vibratome 3000 Plus sectioning System (St Louis, Missouri, USA). The guidelines of the National Institutes of Health for the Care and Use of Laboratory Animals were followed for all experimental procedures.

HRP immunocytochemistry

Monoclonal antibodies against CB and PV were obtained from Sigma-Aldrich (St Louis, Missouri, USA). A monoclonal antibody against CR was obtained from Millipore (Bedford, Massachusetts, USA). The primary antiserum was diluted 1:500, and the biotinylated secondary antiserum was diluted 1:200. Standard immunocytochemical techniques and methods were used, as described previously [26]. As a negative control, some sections were incubated in the same solution without the addition of the primary antibody. These control tissues showed no CB, CR, or PV immunoreactivity (Fig. 1). The tissues were examined and photographed on a Zeiss Axioplan microscope (Carl Zeiss Meditec Incorporation, Jena, Germany), using conventional or differential interference contrast (DIC) optics.

Fluorescence immunocytochemistry

Monoclonal and polyclonal antibodies against CB, CR and PV were used in this study. Monoclonal antibodies against CB and PV, and a polyclonal antibody against CB, were obtained from Sigma-Aldrich. Monoclonal antibodies against GABA and CR, and polyclonal antibodies against CR and PV were obtained from Millipore. The primary antisera were diluted in the range 1:500 to 1:1000 (CB, CR, and PV) and 1:250 (GABA). The secondary antibodies used for immunofluorescence included fluorescein (FITC)-conjugated anti-rabbit IgG (Vector Laboratories, Burlingame, California, USA) for detecting the anti-CB, CR, and PV antibodies, and Cy3-conjugated anti-mouse IgG (Jackson ImmuoResearch, West

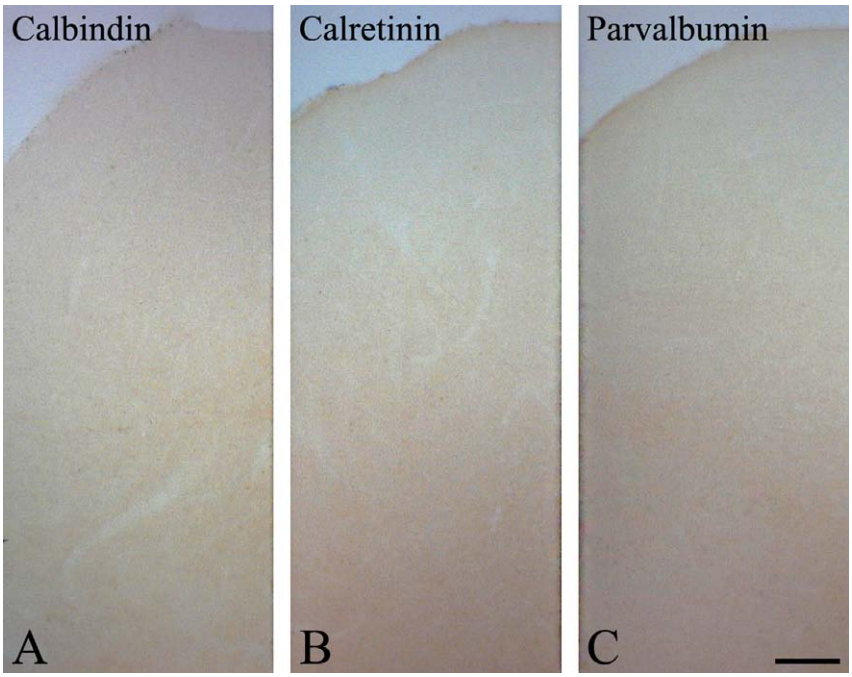

Fig. 1. Low-power photomicrographs of control sections of the bat SC used to show the specificity of CB (**A**), CR (**B**) and PV (**C**). Bar=100 μm.

Grove, Pennsylvania, USA) for detecting the anti-GABA antibody. The same secondary antibodies were used for double-immunofluorescence among the CBPs. Labeled sections were mounted in the Vectashield mounting medium (Vector Laboratories). Images were obtained and viewed with a Zeiss LSM700 laser scanning confocal microscope (Carl Zeiss Meditec Incorporation).

Quantitative analysis

The average diameter and area of labeled cells were computed using a digital camera, Zeiss AxioCam HRc (AxioVison 4; Carl Zeiss Meditec Incorporation). For each of 2 animals, we analyzed the 5 best-labeled sections, each 500 μm in width across the superior-inferior extent of the SC. The fields were positioned in the central SC. A cursor was moved manually around the outer contour of each cell using the digital camera. Analysis was performed using a 40× Zeiss Plan-Apochromat objective. To obtain the best images, we analyzed cells using differential interference contrast (DIC) optics. Only cells containing a nucleus with a nucleolus that was at least faintly visible were included in the analysis.

To determine the number of double-labeled cells, we counted fields 93 μm in width across the superior-inferior extent of the SC from nine different sections selected from three different animals. The fields were positioned in the central SC. Double-labeled images were obtained and viewed with a Zeiss LSM700 laser scanning confocal microscope (Carl Zeiss Meditec Incorporation) using a 40× objective.

III. Results

CBP-IR cells were selectively distributed in the bat SC

Anti-CB-IR cells formed a laminar tier within the upper SGL. This tier of IR cells in the upper SGL could be seen throughout the rostrocaudal extent of the SC. The thickness of this tier at the central portion of the mid-colliculus was approximately 200 μm when measured perpendicular to the pial surface. Virtually all of the cells in the upper SGL were small, and IR cells were rarely found in the other layers (Fig. 2B).

CR-IR cells were widely distributed within the lower SGL and OL, forming a loose tier that was not as distinct as the tier of CB-IR cells. However, this tier was also seen throughout the rostrocaudal extent of the SC. The tier was about 300 μm wide at the central portion of the mid-colliculus. Scattered CR-IR cells were also found within the IGL, IWL, and DGL. Cells in the IGL and DGL included many larger cells (Fig. 2C).

In contrast, PV-IR cells formed a laminar tier within the lower SGL and upper OL. Most cells in this tier were small in size. This tier was approximately 200 μm wide at the central portion of the mid-colliculus. Scattered PV-IR cells were also found throughout intermediate layers, but without a specific laminar pattern. The IGL and IWL contained larger cells (Fig. 2D).

Morphology of anti-CBP-IR cells

CB immunoreactivity was found in certain small- to medium-sized cells in the upper SGL of the bat SC. The principal neuronal cell type that was labeled with antibody

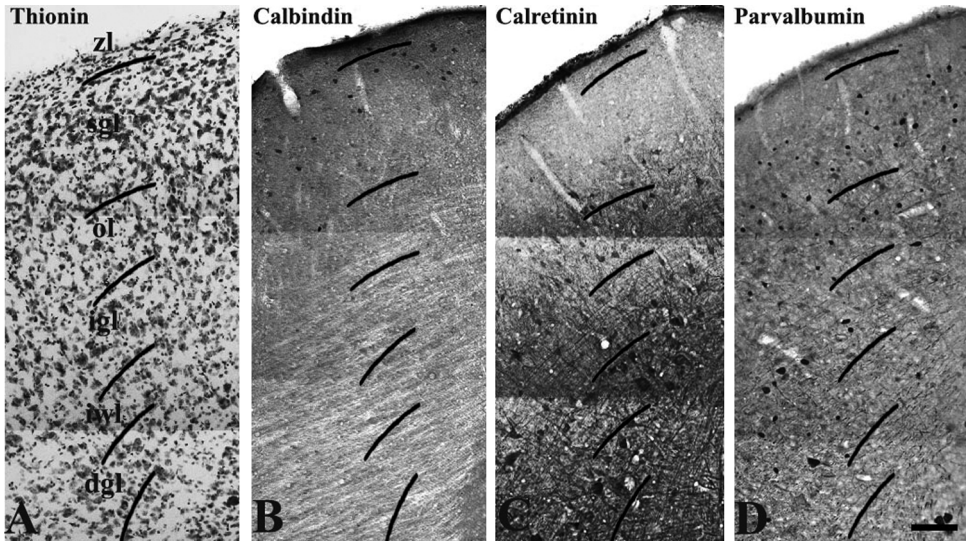

Fig. 2. Low-power photomicrographs of the laminar distribution of CB-, CR-, and PV-IR cells in the bat SC. (**A**) Thionin-stained section showing collicular lamination. (**B**) CB-IR cells in normal bat SC, distributed within the ZL and the upper SGL. (**C**) CR-IR cells in normal bat SC, distributed within the lower SGL and OL. The majority of CR-IR cells were distributed from the lower IGL to the DGL. (**D**) PV-IR cells in normal bat SC, distributed in the lower SGL and upper OL. Scattered PV-IR cells were also distributed in intermediate layers. ZL, zonal layer; SGL, superficial gray layer; OL, optic layer; IGL, intermediate gray layer; IWL, intermediate white layer; DGL, deep gray layer. Bar=100 μm.

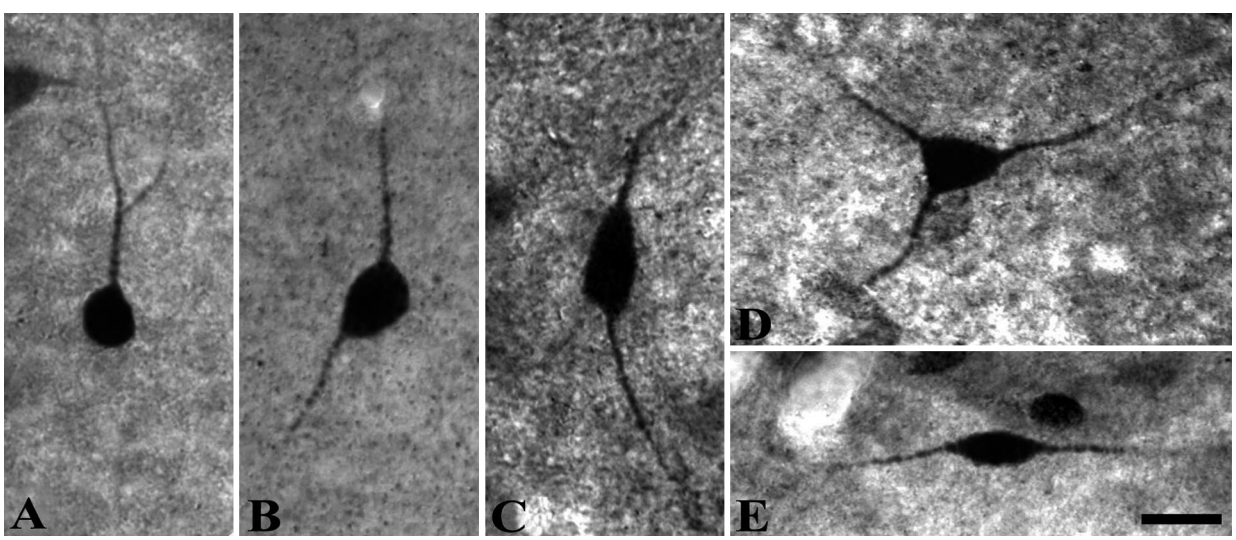

Fig. 3. High-power differential interference contrast photomicrographs of CB-IR cells in the bat SC. (**A**) A small-sized oval cell. (**B**) An oval cell. (**C**) A vertical fusiform cell with a vertical fusiform cell body and two processes poining toward the pial surface and inward. (**D**) A multipolar stellate cell with a polygonally-shaped cell body. (**E**) A horizontal cell with a horizontal fusiform cell body with horizontally-oriented processes. Bar=20 μm.

against CB in the upper SGL was round or oval in shape. Figure 3 shows representative CB-IR cells in the upper SGL. Figure 3A shows a small-sized oval cell, while Figure 3B shows another oval cell. Figure 3C shows a vertical fusiform cell with a vertical fusiform cell body that has a main process ascending towards the pial surface, as well as a descending process. Stellate cell, as illustrated in Figure 3D has polygonally-shaped cell body with several dendrites coursing in various directions. Figure 3E shows a horizontal cell with a horizontally-oriented small, fusiform cell body and horizontally-oriented processes.

CR-IR cells varied in their size and shape, and their size differed dramatically from that of CB-IR cells. Figure 4A shows representative small round or oval cells. Figure 4B and 4C show vertical fusiform cells, with vertical fusiform cell bodies, and a main process ascending towards the pial surface; Figure 4B also shows neuron with a long descending process. Figure 4D shows a large-sized stellate cell with several dendrites coursing in all directions. Figure 4E shows a horizontal cell with a horizontally-oriented small, fusiform cell body and horizontally-oriented processes.

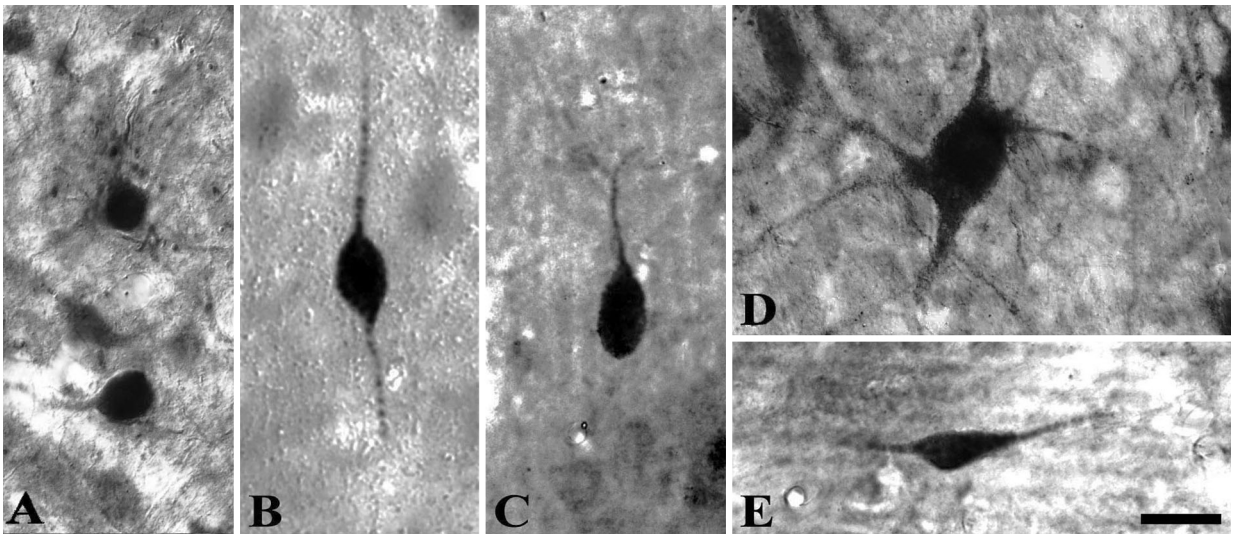

Fig. 4. High-power differential interference contrast photomicrographs of some CR-IR cells in the bat SC. (**A**) Small-sized round or oval cells. (**B**) A vertical fusiform cell with a vertical fusiform cell body and two processes pointing toward the pial surface and inward. (**C**) A vertical fusiform cell that displays a vertical fusiform cell body ascending towards the pial surface. (**D**) A large-sized multipolar stellate cell. (**E**) A horizontal cell with a horizontal thin fusiform cell body and horizontally-oriented processes. Bar=20 μm.

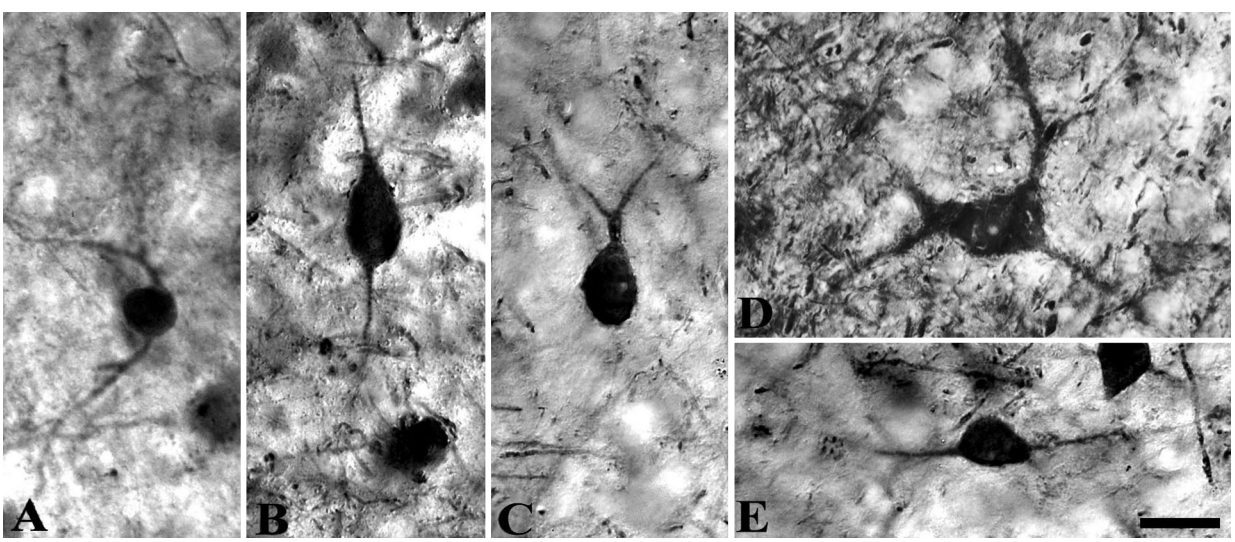

Fig. 5. High-power differential interference contrast photomicrographs of PV-IR cells in the bat SC. (**A**) A small-sized round cell. (**B**) A vertical fusiform cell, with a fusiform cell body, a main process ascending towards the pial surface, and a descending process. (**C**) A pyriform cell with a pyriform cell body and a thick dendrite directed towards the pial surface. (**D**) A large-sized multipolar stellate cell. (**E**) A horizontal cell with a horizontal fusiform cell body and horizontally-oriented processes. Bar=20 μm.

The morphology of many PV-IR cells in the lower SGL and upper OL differed from those in the IGL and IWL, as they were mostly small- to medium-sized round or oval cells. Cells in the IWL and IGL included many stellate cells with multipolar dendrites. However, small- to medium-sized vertical fusiform or pyriform cells with a thick, proximal dendrite directed towards the pial surface were also found. Figure 5A shows a representative small round cell, while Figure 5B shows a vertical fusiform cell with a vertical fusiform cell body, a main process ascending towards the pial surface, and a descending process. Pyriform cells (Fig. 5C) have a vertical fusiform or pyriform cell body with a thick proximal dendrite directed towards the pial surface. Stellate cell (Fig. 5D) has polygonally-shaped cell body with several dendrites coursing in various directions. Figure 5E shows a rare horizontal cell with horizontally-oriented dendrites and a horizontally-oriented fusiform cell body.

The average diameter of 186 CB-IR cells ranged from 9.77 to 14.09 μm, with a mean of 11.59 μm (standard deviation, S.D.=1.08). All cells were small in size (<15.00 μm). The size of CR-IR cells differed considerably from that of

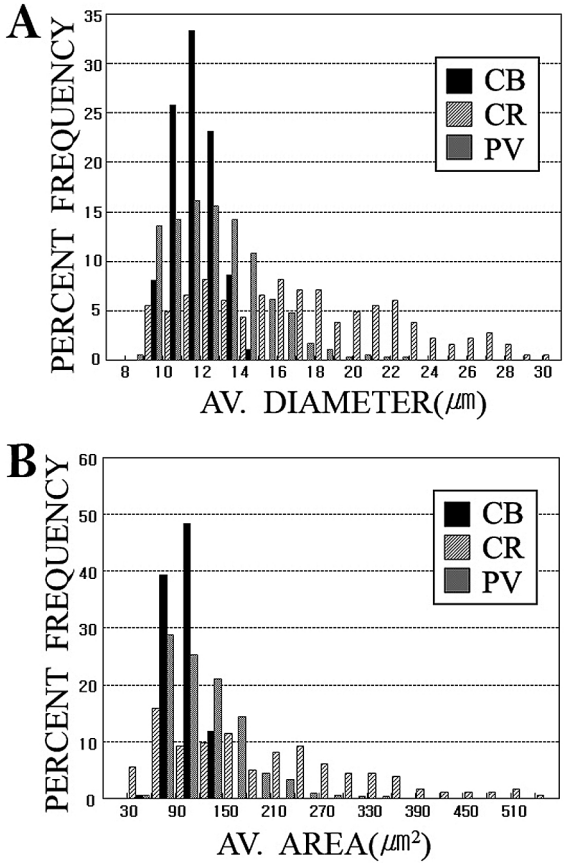

Fig. 6. Histogram showing the percent frequency of cells with respect to average diameter (**A**) and average area of cells (**B**) labeled with CB, CR, and PV in the bat SC.

CB-IR cells; the average diameter of 191 CR-IR cells had a range of 8.01 to 35.96 μm with a mean of 17.17 μm (S.D.=5.50), while that of 360 PV-IR cells ranged from 8.55 to 22.23 μm with a mean of 12.60 μm (S.D.=2.37) (Fig. 6).

The average area of the 186 CB-IR cells was 95.26 μm^2 (S.D.=19.05) with a range of 37.00 to 143.93 μm^2, that of the 191 CR-IR cells was 198.74 μm^2 (S.D.=124.30) with a range of 33.85 to 670.66 μm^2, and that of 360 PV-IR cells was 122.27 μm^2 (S.D.=47.82) with a range of 53.42 to 352.22 μm^2 (Fig. 6).

Co-localization of CBPs and GABA

To determine whether CB, CR, and PV in the bat SC co-localize with GABA, we used fluorescein to detect CBPs and Cy3 to detect GABA. Figure 7A shows cells that were labeled with CB, and Figure 7B shows cells that were labeled with GABA. Figure 7C indicates that there were no cells that were clearly labeled with both CB and GABA in the bat SC. Figure 7D shows cells that were labeled with CR, and Figure 7E shows cells that were labeled with GABA. None of the cells in the SC were clearly labeled with both CR and GABA (Fig. 7F). However, some cells were labeled with PV (Fig. 7G), with GABA (Fig. 7H) or with both PV and GABA (arrowheads in Fig. 7I). Other cells were labeled with either one or the other antibody, but not with both. There was no obvious relationship between cell morphology and single- or double-labeling of the cells.

To estimate the percentage of double-labeled cells, we counted the number of CB-, CR-, or PV-IR cells, and cells double-labeled with GABA, across the layers of the SC in three sections from three animals (9 sections). Quantitatively, no CB- or CR-IR cells were double-labeled with GABA. By contrast, 10.27% of the PV-IR cells were double-labeled with GABA. This percentage of double-labeled cells was relatively consistent across sections and among animals (Table 1).

Co-localization of CB, CR and PV

To determine whether CB, CR, and PV in the bat SC co-localized with each other, we used fluorescein and Cy3 to detect CBPs. Figure 8A and 8D show cells that were labeled with CB, and Figure 8B and 8E show cells that were labeled with CR and PV, respectively. Figure 8C indicates that there were no cells that were clearly labeled with both CB and CR in the bat SC, whereas there were some cells (arrowheads) (approximately 30% of CB-IR cells) that were clearly labeled with both CB and PV (Fig. 8F). Figure 8G shows cells that were labeled with CR, and Figure 8H shows cells that were labeled with PV. As shown in Figure 8I, many cells in the SC were labeled with both CR and PV, and the percentage of PV-IR cells was approximately 90% of CR-IR cells. Compared to the pattern of co-localization between CB and PV, the number of cells labeled with both CR and PV were much more than the cells with CB and PV. Other cells were labeled with either one or the other antibody, but not with both. There was no obvious relationship between cell morphology and single- or double-labeling of the cells.

IV. Discussion

The results of the current study indicate that the expression of CB-, CR-, and PV-IR cells is substantially segregated and localized to specific areas of the bat SC.

At least one definite conclusion can be drawn from these results: the distribution pattern of CB-IR cells is strikingly different from that seen in any animals studied so far. CB-IR cells exhibit a distinct distribution pattern in the mammalian SC that has been previously well described as being generally distributed in 3 tiers. This is strikingly different from the bat SC, where there is only 1 tier. For example, CBs in the cat SC are found within the upper half of the superficial layer, with a second tier bridging the deep OL and IGL, and a third tier within the DGL [43]. Similar results have been found for SCs of monkeys, rabbits, rats, and hamsters [8, 17, 33, 39, 42, 44, 53]. The dog also has 3 tiers of CB-IR cells in the SC, but the distribution of this protein in the superficial SC also differs from that of previously studied animals, as the first tier of CB-IR cells is

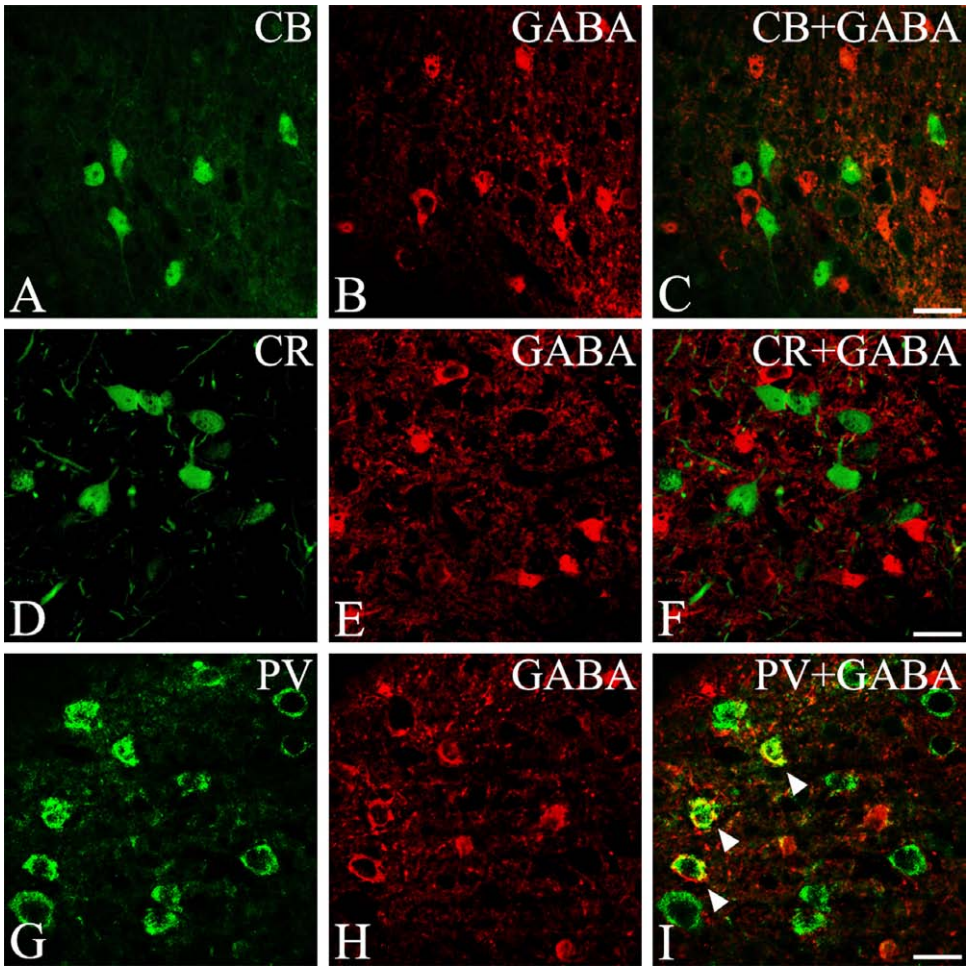

Fig. 7. Fluorescence confocal photomicrographs of the bat SC immunostained for CB (**A**), CR (**D**), PV (**G**), GABA (**B, E, H**), and superimposed images of CBPs and GABA (**C, F, I**). None of the CB- and CR-IR cells double-labeled with GABA. However, some PV-IR cells are double-labeled with GABA in the bat SC (arrowheads). Bar=20 μm.

Table 1. *Percentage of CBP-IR cells and cells double-labeled with GABA in the bat SC*

Antibodies	No. Sections	No. cells	No. Double-labeled	% Double-labeled (Mean±S.D.)
Calbindin D28K	3	19	0	0±0
	3	15	0	0±0
	3	17	0	0±0
Total	9	51	0	0
Calretinin	3	49	0	0±0
	3	59	0	0±0
	3	50	0	0±0
Total	9	158	0	0
Parvalbumin	3	68	8	11.76±1.26
	3	122	13	10.66±0.46
	3	141	13	9.03±1.75
Total	9	331	34	10.27

found in the lower SGL instead of the upper SGL. Nonetheless, all other animals studied so far have 3 tiers of CB-IR cells in the SC, whereas the bat has only 1 tier. In the bat SC, the first tier in the upper SGL is present, but the second and the third tiers, which are present in other animals, are not. These results indicate that there are considerable differences between species in the distribution of CB-IR cells in the SC.

With respect to the distribution of CR-IR cells, once again, at least one definitive conclusion can be drawn from the current study: the CR-IR distribution pattern is different from that seen in any animals studied so far. The antibody

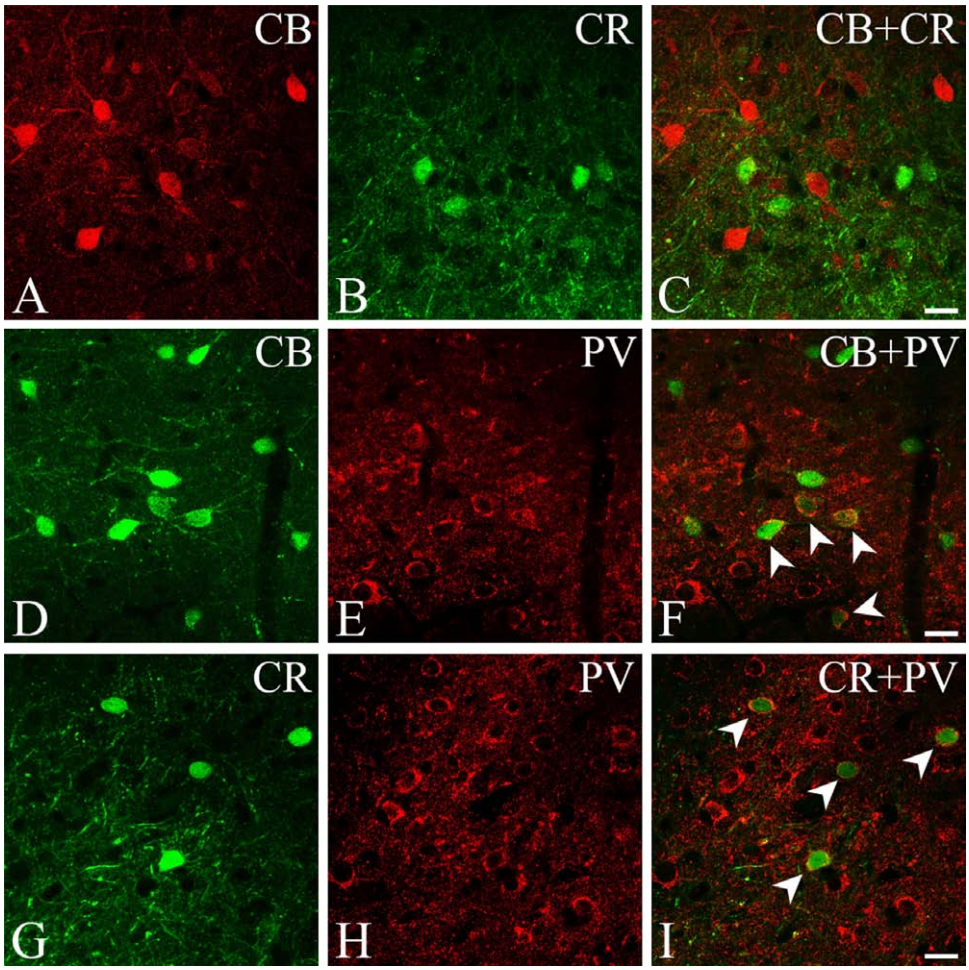

Fig. 8. Fluorescence confocal photomicrographs of the bat SC immunostained for CB (**A, D**), CR (**B, G**), and PV (**E, H**). **C**, **F**, and **I** are superimposed images in CB and CR, CB and PV, and CR and PV, respectively. Some cells (arrowheads) in (**F**) and (**I**) are clearly labeled with both antibodies in the bat SC. Bar=20 μm.

against CR labels a dense plexus of fibers in the superficial layers of the SC in many mammalian species, including the human [40], monkey [57], dog [37], cat [26], rat [3], mouse [15], and hamster [33], while the bat did not display a dense plexus of CR-IR fibers in the superficial layers. In the human SC, CR-IR cells in the deep layers form a broad band in the IGL and DGL [39]. In the dog SC, the neurons of the IGL form clusters [37], whereas in monkey SC, CR-IR cells in the deeper layers do not form any clusters and cells are scattered [57]. The scattered pattern of CR-IR cells in the deep layers of the bat SC is similar to that of the monkey. These results suggest that there are also important differences in CR distribution among animals. However, the distribution pattern of PV-IR cells in the bat SC is similar to that of many other mammalian SCs. In the cat [45], rabbit [17], rat [12], and hamster SC [48], PV-IR cells are concentrated in a tier within the lower SGL and upper OL, while scattered PV-IR cells are found within the deep layers of the SC.

The reason for the different distribution patterns of CB- and CR-IR cells in the bat has not yet been established. This difference suggests, however, that there are diverse functional needs associated with different visual behavioral contexts. These current results draw attention to the importance of studying the neurochemical cytoarchitecture of a diverse selection of animals. Functionally, neurons in superficial layers are concerned with vision, while the deeper SC has a role in integrating sensory information with motor signals, allowing for head orientation and saccadic eye movements [27]. The distinct laminar segregation of CBP-IR cells in the bat SC suggests that a relatively high density of calcium channels exist in various layers of the bat SC. The CB-IR cells in the upper SGL appear to be associated with visual retinal input, while PV-IR cells in the lower SGL are associated with visual cortical input. CR- and PV-IR cells in the deep layers of the bat SC deal with the integration of multiple behaviors related to sensory orientation that are involved in calcium buffering and/or calcium-mediated signal transduction. A preferential loss of PV-IR cells in the intermediate layers, a presumptive multisensory population that targets premotor areas of the brainstem and spinal cord, disrupts the multisensory responses

of the cat SC [9]. However, in spite of the abundance of CBP-expressing cells, there is not much electrophysiological data to delineate the specific role of this protein in the SC. The heterogeneity and differential localization of the CBP-IR cells in the bat SC suggest that these cells operate under a variety of functional contexts. Further studies of the metabolic characteristics of CBPs in the SC will yield a greater understanding of the visual and visuo-motor integration system.

In the current study, the presence of numerous small-sized round or oval CB-IR cells in the upper SGL, and PV-IR cells in the lower SGL and upper OL, suggests that many of these cells may be interneurons, while many PV-IR cells in the deep layers may also be projection neurons. The presence of numerous CR-IR large-sized stellate cells in the deep layers suggests that many of these cells may be projection neurons. In the cat SC, most CB-IR neurons are interneurons, while most of PV-IR neurons are projection neurons [43, 45]. However, opposing data for the cat has also been reported. Thus, it is likely that most CB-IR cells in the rat are projection neurons, while PV-IR neurons in the rat are either primarily interneurons or descending projection neurons [36]. These differences between species imply that there may be functional differences in CBPs among species. Backfilling of the CBP-IR SC cells with a tracer would determine whether CBP-IR cells in the bat SC are projection neurons. In the cat and dog SC, some cells are IR for both CB and GABA [38, 43]. This indicates that these CB-IR cells are GABAergic interneurons in the current study, which is in agreement with studies conducted on the hamster SC [8]. The current results also demonstrate that none of the CR-IR cells in the bat SC is GABAergic neurons, which is in agreement with our previous study where no CR-IR cells were also labeled with an antibody to GABA in the dog SC. In the present study, some PV-IR cells were shown to be GABAergic, and a previous study demonstrated that PV-IR cells in the rat SC were a subset of GABAergic cells [36]. However, the reasons for the differential expression patterns of CBP in GABAergic cells among various SCs are not well understood now.

In the present study, double-immunofluorescence revealed that there were no cells labeled with both CB and CR. This result indicates that CB and CR may not share common functional characteristics in the bat SC, similar to previous studies in hamster [33] and rabbit [29] SCs and rat visual cortex [16]. In rabbit SC in particular, there were no cells in the superficial layer labeled with both CB and CR, whereas some cells in the deep layer co-localized both [29, 47]. In the present study, some cells were labeled with CB and PV in bat SC. In contrast to our study, there were no cells that were labeled with CB and PV in cat SC [45]. Additionally, many CR-IR cells were double-labeled with PV. The human visual cortex also has small populations of cells that double-stain for CR and PV [40]. However, no overlap between CR and PV in the hamster SC and other brain areas, such as the rat visual cortex [16], has been demonstrated. The results of the previous and present studies indicate that there are considerable differences not only between species but also between areas in same animals.

Although the presence of CBPs is common in many neuronal cells, and they are thought to play a substantial role in buffering intracellular calcium levels, the exact function of CBPs remains unclear. Recent studies have elucidated some important functions of CBPs in the central nervous system, such as protecting dopaminergic neurons from apoptosis, and age-related memory deficits [6, 59]. CR inputs are important for the motor neurons that cause upward eye movements [63], and for balancing enhanced excitatory input in rat hippocampus circuits [1]. PV plays an important role in protecting cells from calcium overload [24] and is associated with experience-induced plasticity, thereby regulating adult learning [13]. Impaired regulation of calcium uptake by CBPs is closely related to many neurodegenerative processes [7, 23, 34, 49, 52] such as Alzheimer's disease [4, 14, 41], Parkinson's disease [28], Niemann-Pick disease [10], and amyotrophic lateral sclerosis [21]. The exact functions of each of the CBPs in collicular cells remain unknown, although the characteristic laminar organization and heterogeneity of IR cells in the present study suggest that these CBPs play a variety of roles in bat collicular physiology. Further detailed investigations of the function of each CBP are necessary to elucidate these issues.

V. Acknowledgments

This research was supported by Basic Science Research Program through the National Research Foundation of Korea (NRF) funded by Ministry of Education (NRF-2010-0003717). We thank the Language Institute of Kyungpook National University and Cactus Communications, Korea for proofreading the manuscript.

VI. References

1. Abuhamed, M. M., Bo, X., Alsharafi, W. A., Jing, L., Long, L., Zhiguo, W. and Zhi, S. (2010) Changes in the numbers and distribution of calretinin in the epileptic rat hippocampus. *Neurosciences (Riyadh)* 15; 159–166.
2. Altringham, J. (1998) Bats: Biology and Behaviour. Oxford University Press, New York, USA.
3. Arai, M., Arai, R., Sasamoto, K., Kani, K., Maeda, T., Deura, S. and Jacobowitz, D. M. (1993) Appearance of calretinin-immunoreactive neurons in the upper layers of the rat superior colliculus after eye enucleation. *Brain Res.* 613; 341–346.
4. Baglietto-Vargas, D., Moreno-Gonzalez, I., Sanchez-Varo, R., Jimenez, S., Trujillo-Estrada, L., Sanchez-Mejias, E., Torres, M., Romero-Acebal, M., Ruano, D., Vizuete, M., Vitorica, J. and Gutierrez, A. (2010) Calretinin interneurons are early targets of extracellular amyloid-beta pathology in PS1/AbetaPP Alzheimer mice hippocampus. *J. Alzheimers Dis.* 21; 119–132.
5. Baimbridge, K. G., Celio, M. R. and Rogers, J. H. (1992) Calcium-binding proteins in the nervous system. *Trends Neurosci.* 15; 303–308.

6. Barinka, F., Salaj, M., Rybář, J., Krajčovičová, E., Kubová, H. and Druga, R. (2012) Calretinin, parvalbumin and calbindin immunoreactive interneurons in perirhinal cortex and temporal area Te3V of the rat brain: Qualitative and quantitative analyses. *Brain Res.* 1436; 68–80.
7. Barraclough, R. (1998) Calcium-binding protein S100A4 in health and disease. *Biochem. Biophys. Acta* 1448; 190–199.
8. Behan, M., Jourdain, A. and Bray, G. M. (1992) Calcium binding protein (calbindin D28k) immunoreactivity in the hamster superior colliculus: ultrastructure and lack of co-localization with GABA. *Exp. Brain Res.* 89; 115–124.
9. Burnett, L. R., Stein, B. E., Chaponis, D. and Wallace, M. T. (2004) Superior colliculus lesions preferentially disrupt multisensory orientation. *Neuroscience* 124; 535–547.
10. Byun, K., Kim, D., Bayarsaikhan, E., Oh, J., Kim, J., Kwak, G., Jeong, G. B., Jo, S. M. and Lee, B. (2013) Changes of calcium binding proteins, c-Fos and COX in hippocampal formation and cerebellum of Niemann–Pick, type C mouse. *J. Chem. Neuroanat.* 52; 1–8.
11. Celio, M. R. (1990) Calbindin D-28k and parvalbumin in the rat nervous system. *Neuroscience* 35; 375–475.
12. Cork, R. J., Baber, S. Z. and Mize, R. R. (1998) Calbindin D28k- and parvalbumin-immunoreactive neurons form complementary sublaminae in the rat superior colliculus. *J. Comp. Neurol.* 394; 205–217.
13. Donato, F., Rompani, S. B. and Caroni, P. (2013) Parvalbumin-expressing basket-cell network plasticity induced by experience regulates adult learning. *Nature* 504; 272–276.
14. Ferrer-Acosta, Y., Rodríguez-Cruz, E. N., Orange, F., De Jesús-Cortés, H, Madera, B., Vaquer-Alicea, J., Ballester, J., Guinel, M. J., Bloom, G. S. and Vega, I. E. (2013) EFhd2 is a novel amyloid protein associated with pathological tau in Alzheimer's disease. *J. Neurochem.* 125; 921–931.
15. Gobersztejn, F. and Britto, L. R. G. (1996) Calretinin in the mouse superior colliculus originates from retinal ganglion cells. *Braz. J. Med. Biol. Res.* 29; 1507–1511.
16. Gonchar, Y. and Burkhalter, A. (1997) Three distinct families of GABAergic neurons in rat visual cortex. *Cereb. Cortex* 7; 347–358.
17. González-Soriano, J., González-Flores, M. L., Contreras-Rodríguez, J., Rodríguez-Veiga, E. and Martínez-Sainz, P. (2000) Calbindin D28k and parvalbumin immunoreactivity in the rabbit superior colliculus: an anatomical study. *Anat. Rec.* 259; 334–346.
18. Grantyn, R. (1988) Gaze control through superior colliculus: structure and function. *Rev Oculomot. Res.* 2; 273–333.
19. Hage, S. R. and Metzner, W. (2013) Potential effects of anthropogenic noise on echolocation behavior in horseshoe bats. *Commun. Integr. Biol.* 6; e24753.
20. Harting, I. (2004) Puffs and patches: a brief chronological review. In "The Superior Colliculus: New Approaches for Studying Sensorimotor Integration", ed. by W. C. Hall, A Moschovakis, CRC Press LLC, Florida, USA, pp. 83–105.
21. Hayashi, S., Amari, M. and Okamoto, K. (2013) Loss of calretinin- and parvalbumin-immunoreactive axons in antero-lateral columns beyond the corticospinal tracts of amyotrophic lateral sclerosis spinal cords. *J. Neurol. Sci.* 331; 61–66.
22. Heizmann, C. W. (1984) Parvalbumin, an intracellular calcium-binding protein; distribution, properties and possible roles in mammalian cells. *Experientia* 40; 910–921.
23. Heizmann, C. W. and Braun, K. (1995) Calcium Regulation by Calcium-binding Proteins in Neurodegenerative Disorders, Springer-Verlag, New York.
24. Hipólito-Reis, J., Pereira, P. A., Andrade, J. P. and Cardoso, A. (2013) Prolonged protein deprivation differentially affects calretinin- and parvalbumin-containing interneurons in the hippocampal dentate gyrus of adult rats. *Neurosci. Lett.* 555; 154–158.
25. Holland, R. A., Waters, D. A. and Rayner, J. M. (2004) Echolocation signal structure in the Megachiropteran bat *Rousettus aegyptiacus* Geoffroy 1810. *J. Exp. Biol.* 207; 4361–4369.
26. Hong, S.-K., Kim, J.-Y. and Jeon, C.-J. (2002) Immuno-cytochemical localization of calretinin in the superficial layers of the cat superior colliculus. *Neurosci. Res.* 44; 325–335.
27. Huerta, M. F. and Harting, J. K. (1984) The mammalian superior colliculus: studies of its morphology and connections. In "The Comparative Neurology of the Optic Tectum", ed. by H. Vanega, Plenum Press, New York, pp. 687–772.
28. Hurley, M. J., Brandon, B., Gentleman, S. M. and Dexter, D. T. (2013) Parkinson's disease is associated with altered expression of CaV1 channels and calcium-binding proteins. *Brain* 136; 2077–2097.
29. Jeon, C.-J., Pyun, J.-K. and Yang, H.-W. (1998) Calretinin and calbindin D28K immunoreactivity in the superficial layers of the rabbit superior colliculus. *Neuroreport* 9; 3847–3852.
30. Jeon, Y.-K., Kim, T.-J., Lee, J.-Y., Choi, J.-S. and Jeon, C. J. (2007) AII amacrine cells in the inner nuclear layer of bat retina: identification by parvalbumin immunoreactivity. *Neuroreport* 18; 1095–1099.
31. Jones, G. and Rayner, J. M. V. (1989) Foraging behavior and echolocation of wild horseshoe bats Rhinolophus ferrumequinum and R. hipposideros (Chiroptera, Rhinolophidae). *Behav. Ecol. Sociobiol.* 25; 183–191.
32. Jones, G. and Siemers, B. M. (2011) The communicative potential of bat echolocation pulses. *J. Comp. Physiol. A Neuroethol. Sens. Neural. Behav. Physiol.* 197; 447–457.
33. Kang, Y.-S., Park, W.-M., Lim, J.-K., Kim, S.-Y. and Jeon, C. J. (2002) Changes of calretinin, calbindin D28K and parvalbumin immunoreactive neurons in the superficial layers of the hamster superior colliculus following monocular enucleation. *Neurosci. Lett.* 330; 104–108.
34. Kim, J.-E., Kwak, S.-E., Kim, D.-S., Won, M.-H., Kwon, O.-S., Choi, S.-Y. and Kang, T.-C. (2006) Reduced calcium binding protein immunoreactivity induced by electroconvulsive shock indicates neuronal hyperactivity, not neuronal death or deactivation. *Neuroscience* 137; 317–326.
35. Kim, T.-J., Jeon, Y.-K, Lee, J.-Y, Lee, E.-S. and Jeon, C.-J. (2008) The photoreceptor populations in the retina of the greater horseshoe bat Rhinolophus ferrumequinum. *Mol. Cells* 26; 373–379.
36. Lane, R. D., Allan, D. M., Bennett-Clarke, C. A., Howell, D. L. and Rhoades, R. W. (1997) Projection status of calbindin- and parvalbumin-immunoreactive neurons in the superficial layers of the rat's superior colliculus. *Vis. Neurosci.* 14; 277–286.
37. Lee, J.-Y., Choi, J.-S., Ahn, C.-H., Kim, I.-S., Ha, J.-H. and Jeon, C.-J. (2006) Calcium-binding protein calretinin immunoreactivity in the dog superior colliculus. *Acta Histochem. Cytochem.* 39; 125–138.
38. Lee, J.-Y., Choi, J.-S., Ye, E.-A., Kim, H.-H. and Jeon, C.-J. (2007) Organization of calbindin D28K-immunoreactive neurons in the dog superior colliculus. *Zoolog. Sci.* 24; 1103–1014.
39. Leuba, G. and Saini, K. (1996) Calcium-binding proteins immunoreactivity in the human subcortical and cortical visual structures. *Vis. Neurosci.* 13; 997–1009.
40. Leuba, G. and Saini, K. (1997) Co-localization of parvalbumin, calretinin, and calbindin D-28k in human cortical and subcortical visual structures. *J. Chem. Neuroanat.* 13; 41–52.
41. Leuba, G., Kraftsik, R. and Sainin, K. (1998) Quantitative distribution of parvalbumin, calretinin, and calbindin D28K immunoreactive neurons in the visual cortex of normal and Alzheimer cases. *Exp. Neurol.* 152; 278–291.

42. McHaffie, J. G., Anstrom, K. K., Gabriele, M. L. and Stein, B. E. (2001) Distribution of the calcium-binding proteins calbindin D-28K and parvalbumin in the superior colliculus of adult and neonatal cat and rhesus monkey. *Exp. Brain Res.* 141; 460–470.
43. Mize, R. R., Jeon, C. J., Butler, G. D., Luo, Q. and Emson, P. C. (1991) The calcium binding protein calbindin-D28K reveals subpopulations of projection and interneurons in the cat superior colliculus. *J. Comp. Neurol.* 307; 417–436.
44. Mize, R. R. and Luo, Q. (1992) Visual deprivation fails to reduce calbindin 28 kD or GABA immunoreactivity in the rhesus monkey superior colliculus. *Vis. Neurosci.* 9; 157–168.
45. Mize, R. R., Luo, Q., Butler, G., Jeon, C. J. and Nabors, B. (1992) The calcium binding protein parvalbumin and calbindin-D28K form complementary patterns in the cat superior colliculus. *J. Comp. Neurol.* 320; 243–256.
46. Neuweiler, G. (1990) Auditory adaptations for prey capture in echolocating bats. *Physiol. Rev.* 70; 615–641.
47. Park, W.-M., Kang, Y.-S., Pyun, J.-K., Jeon, Y.-K. and Jeon, C.-J. (2000) Distribution and Morphology of calretinin and calbindin D28K containing neurons in the deep layers of the rabbit superior colliculus. *Exp. Neurobiol.* 9; 61–77.
48. Park, W.-M., Kim, M.-J. and Jeon, C.-J. (2004) Ionotropic glutamate receptor GluR2/3-immunoreactive neurons in the cat, rabbit, and hamster superficial superior colliculus. *Neurosci. Res.* 49; 139–155.
49. Polans, A., Baehr, W. and Palczewski, K. (1996) Turned on by Ca^{2+}! The physiology and pathology of Ca^{2+}-binding proteins in the retina. *Trends Neurosci.* 19; 547–554.
50. Reynolds, G. P., Zhang, Z. J. and Beasley, C. L. (2001) Neurochemical correlates of cortical GABAergic deficits in schizophrenia: selective losses of calcium binding protein immunoreactivity. *Brain Res. Bull.* 55; 579–584.
51. Rogers, J. H. (1987) Calretinin: a gene for a novel calcium-binding protein expressed principally in neurons. *J. Cell Biol.* 105; 1343–1353.
52. Schäfer, B. W. and Heizmann, C. W. (1996) The S100 family of EF-hand calcium-binding proteins: functions and pathology. *Trends Biochem. Sci.* 21; 134–140.
53. Schmidt-Kastner, R., Meller, D. and Eysel, U. T. (1992) Immunohistochemical changes of neuronal calcium-binding proteins parvalbumin and calbindin-D-28k following unilateral deafferentation in the rat visual system. *Exp. Neurol.* 117; 230–246.
54. Schnitzler, H.-U. and Kalko, E. K. V. (2001) Echolocation by insect-eating bats. *BioScience* 51; 557–569.
55. Schwaller, B. (2007) Emerging functions of the "Ca2+ buffers" parvalbumin, calbindin D-28k and calretinin in the brain. In "Handbook of Neurochemistry and Molecular Neurobiology", ed. by A. Lajtha and N. Banik, Springer-Verlag, Berlin Heidelberg, pp. 198–221.
56. Simmons, J. A. (1973) The resolution of target range by echolocating bats. *J. Acoust. Soc. Am.* 54; 157–173.
57. Soares, J. G., Botelho, E. P. and Gattass, R. (2001) Distribution of calbindin, parvalbumin and calretinin in the lateral geniculate nucleus and superior colliculus in Cebus apella monkeys. *J. Chem. Neuroanat.* 22; 139–146.
58. Studholme, K. M., Yazulla, S. and Phillips, C. J. (1987) Interspecific comparisons of immunohistochemical localization of retinal neurotransmitters in four species of bats. *Brain Behav. Evol.* 30; 160–173.
59. Sun, S., Li, F., Gao, X., Zhu, Y., Chen, J., Zhu, X., Yuan, H. and Gao, D. (2011) Calbindin-D28K inhibits apoptosis in dopaminergic neurons by activation of the PI3-kinase-Akt signaling pathway. *Neuroscience* 199; 359–367.
60. Surlykke, A., Pedersen, S. B. and Jakobsen, L. (2009) Echolocating bats emit a highly directional sonar sound beam in the field. *Proc. R. Soc.* 276; 853–860.
61. Suthers, R. A. (1970) A comment on the role of choroidal papillae in the fruit bat retina. *Vision Res.* 10; 921–923.
62. Welsh, M. J. (1988) Localization of intracellular calcium-binding proteins. In "Calcium Binding Proteins", vol. 2, Biological Functions, ed. by M. P. Thompson, CRC Press, Cleveland, Ohio, pp. 1–19.
63. Zeeh, C., Hess, B. J. and Horn, A. K. (2013) Calretinin inputs are confined to motoneurons for upward eye movements in monkey. *J. Comp. Neurol.* 521; 3154–3166.
64. Zhao, H., Xu, D., Zhou, Y., Flanders, J. and Zhang, S. (2009) Evolution of opsin genes reveals a functional role of vision in the echolocating little brown bat (Myotis lucifugus). *Biochem. Syst. Ecol.* 37; 154–161.